Upconversion in Er^{3+}-dimer systems: Trends within the series $Cs_3Er_2X_9$ (X=Cl,Br,I)

Markus P. Hehlen, Karl Krämer, and Hans U. Güdel
Department of Chemistry, University of Bern, Freiestrasse 3, 3000 Bern 9, Switzerland

Ross A. McFarlane and Robert N. Schwartz
Hughes Research Laboratories, 3011 Malibu Canyon Road, Malibu, California 90265
(Received 8 November 1993)

The dimer compounds $Cs_3Er_2X_9$ (X=Cl,Br,I) were synthesized and grown as crystals. Their f-f absorption spectra were measured and their upconversion luminescence behavior was studied as a function of temperature. Both $^4I_{15/2}\rightarrow{}^4I_{11/2}$ and $^4I_{15/2}\rightarrow{}^4I_{9/2}$ excitations were used. The highest-energy phonons were found by Raman spectroscopy at 285, 190, and 160 cm^{-1} in $Cs_3Er_2X_9$ (X=Cl,Br,I), respectively. The upconversion and cross-relaxation behavior is essentially determined by two factors: (i) As a result of the lower phonon energies multiphonon-relaxation processes are orders of magnitude less competitive than in fluorides; (ii) as a result of their dimeric character with very short intradimer Er^{3+}-Er^{3+} distances and the relatively short interdimer separations all types of nonradiative energy-transfer processes are very competitive. The following trends were observed: a redshift of the f-f multiplet baricenters of up to 1% between chloride and iodide, a reduction of crystal-field splittings up to 50% between chloride and iodide, enhanced near-infrared to visible upconversion efficiency between chloride and bromide or iodide. All these trends are rationalized with simple models. For some selected crystal-field transitions energy splittings resulting from exchange interactions within the dimers were observed.

I. INTRODUCTION

Upconversion, i.e., photoexcitation followed by luminescence at a shorter wavelength, is a ubiquitous phenomenon among insulating compounds containing trivalent rare-earth-metal ions. There is hardly an Er^{3+}-doped oxide or fluoride material which does not exhibit visible luminescence after $^4I_{11/2}$ or $^4I_{9/2}$ excitation around 985 or 810 nm, respectively. Various mechanisms have been discussed to account for the phenomenon, and depending on variables such as host material, concentration, temperature, and mode of excitation, a particular mechanism may become dominant.[1,2] At high rare-earth-ion concentrations a mechanism becomes efficient in which excitation energy is transferred nonradiatively from one excited center to another in close proximity. Thus one center loses energy to upconvert the other. Both exchange and electric multipole-multipole interactions can induce such a process.[3] The most relevant near-infrared (NIR) to visible upconversion processes for Er^{3+} are schematically represented in Fig. 1.

Most of the recent research on upconversion processes in rare-earth compounds has been materials oriented, with a special emphasis on NIR-to-visible upconversion. The ultimate goal is the development of upconversion visible lasers operating at room temperature and being pumped by semiconductor diode lasers in the NIR.[4] For a recent review, see Ref. 5. Er^{3+}-doped crystals and glasses have received a great deal of attention, mainly because of the favorable energy-level structure of Er^{3+}.[5-9] Both the $^4I_{11/2}$ and $^4I_{9/2}$ excitations shown in Fig. 1 are at wavelengths where diode pumping is possible. This wavelength range is also accessible by Ti:sapphire-laser excitation, and most of the research is done with this mode of excitation. Oxide and fluoride hosts have been studied more extensively than other potential host materials. This preference has mainly practical and not scientific reasons. Oxides and to a lesser degree fluorides are chemically inert, they are relatively hard, and can be cut and polished.

From a scientific point of view it is attractive to extend the range of host materials to halides other than fluoride. This will have an effect on the energies of the f-f transitions, on the crystal-field splittings, and on the phonon energies. Since upconversion can critically depend on all of these, we should not be surprised to find different upconversion behavior from that in oxide and fluoride materials. In detailed studies of Er^{3+}-doped $CsCdBr_3$ it has indeed been shown that the excited-state dynamics and the resulting upconversion luminescence spectra are fundamentally different from those of oxide and fluoride lattices.[10,11]

Crystal lattices in which the rare-earth ions occur in pairs are attractive because of the requirement of proximity in the upconversion process discussed above. Pairs can be created by doping trivalent ions into lattices such as $CsMgCl_3$, $CsMgBr_3$, and $CsCdBr_3$.[12] Upconversion studies of Er^{3+} doped into all of these lattices have been reported.[10-12] The present study is devoted to undiluted ternary Er^{3+}-halide compounds with a dimer structure. All three compounds $Cs_3Er_2X_9$ (X=Cl,Br,I) contain $[Er_2X_9]^{3-}$ pairs consisting of two face-sharing distorted octahedra. The dimer structure is shown in Fig. 2. $Cs_3Er_2Cl_9$ and $Cs_3Er_2Br_9$ crystallize in the rhombohedral space group $R\bar{3}c$ (Refs. 13,14) and $Cs_3Er_2I_9$ in the hexagonal space group $P6_3/mmc$.[15] The crystal structures differ only slightly in the stacking sequence of the CsX_3 layers. The point symmetry of Er^{3+} as well as of the

0163-1829/94/49(18)/12475(10)/$06.00

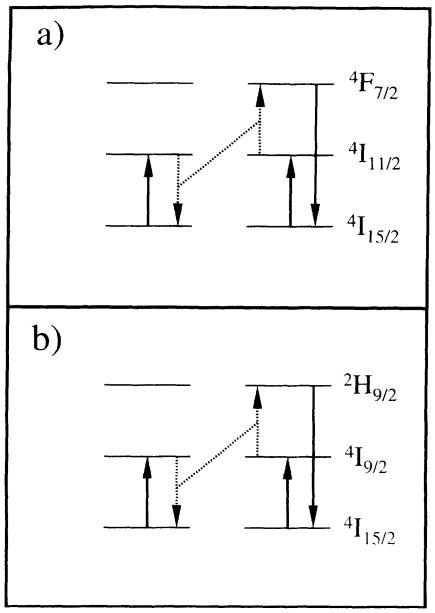

FIG. 1. Schematic representation of the two relevant upconversion processes in $[Er_2X_9]^{3-}$ dimers.

whole $[Er_2X_9]^{3-}$ dimer is C_3 for X=Cl,Br and C_{3v} for X=I. The trigonal dimer axes are parallel to the hexagonal c axis of the lattices. Er^{3+}-Er^{3+} distances within and between neighboring dimers are collected in Table I. The face-sharing arrangement leads to the shortest possible Er^{3+}-Er^{3+} distances within these dimers, and we expect high efficiency for all nonradiative energy-transfer processes such as upconversion and cross relaxation. Evidence for relatively strong exchange interactions within the dimers has been found in the corresponding Tb^{3+}, Dy^{3+}, Ho^{3+}, and Yb^{3+} compounds, all crystallizing in the same crystal structure.[16-18] In addition to electric dipole-dipole induced nonradiative energy-transfer processes, we therefore expect contributions from an exchange mechanism. The dimers are separated by Cs^+ ions, but, as shown in Table I, the shortest interdimer

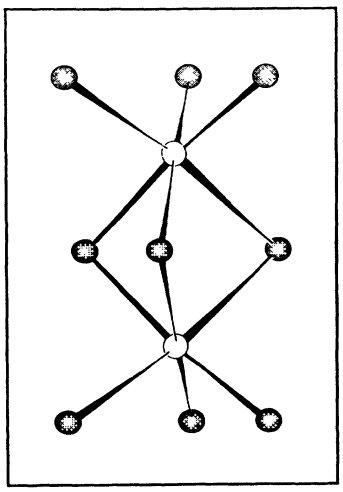

FIG. 2. Dimer structure of $[Er_2X_9]^{3-}$.

TABLE I. Number and distance (Å) of shortest Er^{3+}-Er^{3+} contacts in $Cs_3Er_2X_9$ (X=Cl,Br,I) at room temperature.

	$Cs_3Er_2Cl_9$[a]	$Cs_3Er_2Br_9$[a]	$Cs_3Er_2I_9$[b]
Intradimer	1× 3.625	1× 3.836	1× 4.014
Interdimer	1× 5.522	1× 5.849	
	3× 7.536	3× 7.862	3× 8.166
	3× 7.911	3× 8.265	

[a] $Cs_3Tl_2Cl_9$-type structure (Refs. 13,14).
[b] $Cs_3Cr_2Cl_9$-type structure (Ref. 15).

separations are such that excitation-transfer processes between dimers should still occur with relatively high efficiency. In Er^{3+}-doped $CsCdBr_3$ the separation of the Er^{3+} ions within the dimers is 6.0 Å, and the upconversion processes shown in Figs. 1(a) and 1(b) have been shown to occur at 10 K with rate constants k=128 and 1742 s^{-1}, respectively.[10]

In the present paper we describe and discuss the trends observed in the series $Cs_3Er_2X_9$(X=Cl,Br,I). By using the principle of chemical variation without changing the structure we gain some insight into the dominant radiative and nonradiative processes. In a subsequent paper the upconversion and cross-relaxation processes in $Cs_3Er_2Br_9$ and its diluted analog $Cs_3Lu_2Br_9$:1%Er^{3+} will be discussed in detail.

II. EXPERIMENTAL

A. Synthesis and crystal growth

Dry ErX_3 (X=Cl,Br) were prepared using the NH_4X method.[19] 0.1 mole of Er_2O_3 (Rhone Poulenc, 99.999%) and 0.7 moles of NH_4X (Merck, pro analysi) were dissolved in concentrated HX solution (Merck, Suprapur) and evaporated to dryness. The $(NH_4)_3ErX_6$ obtained were further dried under HX gas (Fluka, 99.8%) at 200 °C for 4 h, followed by decomposition under vacuum at 325 °C for 6 h to obtain ErX_3. CsX (Merck, Suprapur) were also dried under HX gas.

The NH_4X method cannot be used for the iodides, which had to be synthesized starting from the elements.[19,20] A silica ampoule was filled with erbium powder (Johnson-Matthey, 99.9%) and iodine (Merck, resublimed) and sealed off under vacuum. They were heated to 200 °C for 18 h to react to ErI_3. To obtain dry CsI, Cs_2CO_3 (Merck, pro analysi) and NH_4I (Merck, pro analysi) were dissolved in concentrated HI solution (Merck, Suprapur) and evaporated to dryness. In a tantalum boat the product was heated to 410 °C in a stream of argon gas to remove the NH_4I and then melted down under vacuum to obtain CsI.

Starting from CsX and MX_3, crystals of $Cs_3M_2X_9$ were grown in silica ampoules using the Bridgman technique. Due to the hygroscopic nature of all these compounds, syntheses and sample handling had to be carried out in a dry inert atmosphere.

B. Spectroscopic measurements

Single crystals were mounted in resin (Buehler Castrolite) from which a plate was cut using a diamond saw. The sample was ground and polished using Al_2O_3 powders of decreasing size down to 0.3 μm and then mounted in a closed copper cell which was used for the 13-K optical-absorption measurements in a closed-cycle cryostat. Crystals for Raman, luminescence, and excitation experiments were sealed in quartz ampoules under 400 mbar helium pressure to insure sufficient thermal contact with the cooling medium. Sample cooling was achieved using a helium gas-flow technique. Raman, luminescence, and excitation measurements were done on randomly oriented crystals.

Polarized absorption spectra were recorded on a Cary 5E (Varian) spectrometer. The instrumental resolution was typically 0.1 nm in the visible-UV and 0.2 nm in the IR spectral region.

Upconversion luminescence spectra obtained under cw excitation were measured at temperatures between 5 K and room temperature. Excitation was provided by two Ti:sapphire lasers (Schwartz Electrooptics) operating either in the vicinity of 810 nm to pump the $^4I_{9/2}$ multiplet of Er^{3+}, or near 980 nm to pump $^4I_{11/2}$. The laser power was attenuated to 100 mW and the beam was focused onto the crystal ($f=150$ mm). A Hilger 1-m Czerny-Turner monochromator driven by a computer-controlled stepper motor was employed for spectral analysis using a Hamamatsu R639 GaAs-photocathode detector. A light chopper preceded the monochromator input slit and a lock-in amplifier was used to measure the photomultiplier output. The signal was then digitized and subsequent data analysis was accomplished using IGOR.[21]

In order to compare signal intensities over the scanned wavelength region, it is necessary to compensate for the variation in the transmission efficiency of the monochromator and for the sensitivity of the photomultiplier. Using a 3200-K tungsten-halogen lamp as a source having a known spectral content, this dependence was measured between 300 and 1000 nm, and a correction factor determined that was applied to the measured spectral data.

For most of the survey spectra, slit widths of 500 μm were chosen, corresponding to a spectral bandwidth of about 5 Å. This was reduced to about 1 Å by lowering the slit width for the highly resolved spectra.

Upconversion excitation spectra were measured using a multimode Ti:sapphire laser (Schwartz Electrooptics) in standing-wave configuration with a spectral bandwidth of about 1 cm^{-1} at 980 nm. Wavelength control was achieved by an inchworm-driven (Burleigh PZ-501) birefringent filter and a wavemeter (Burleigh WA2100). The sample luminescence was dispersed by a 0.85-m double monochromator (Spex 1402) and detected by a cooled photomultiplier (RCA 31034) using a photon-counting system (Stanford Research SR 400). No correction was made for the wavelength dependence of the Ti:sapphire-laser output over the spectral range 960–990 nm.

Raman spectra were excited at 590.6 nm with linearly polarized light from an argon-ion laser pumped dye laser. In order to eliminate luminescence from Er^{3+} ions the dye laser was tuned to a wavelength where Er^{3+} absorption is a minimum. Light scattered through 90° was passed through a 0.6-m triple-stage spectrometer (Spex 1877) and detected with a cooled Hamamatsu R928 photomultiplier. The output signal was processed with EG&G Ortec photon-counting electronics. The spectrometer drive controller (CD2A Compudrive) and the photon-counting electronics were interfaced to a PC for data acquisition and control. The slits on the spectrometer stage of the triple monochromator were set at 200 μm, which corresponds to an instrumental resolution of approximately 8 cm^{-1}.

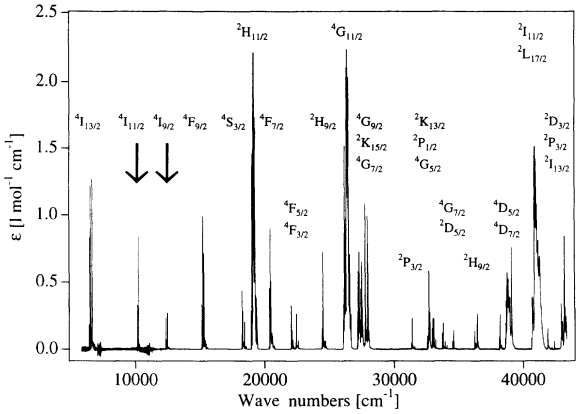

FIG. 3. Unpolarized survey absorption spectrum of a $Cs_3Er_2Cl_9$ crystal at 13 K. Excited states are labeled, and the two states used for upconversion excitation are marked by arrows.

III. RESULTS

Figure 3 shows the unpolarized absorption spectrum of a $Cs_3Er_2Cl_9$ crystal at 13 K in the NIR-to-UV region. The sharp and relatively weak f-f transition multiplets are readily assigned as shown in the figure. The $Cs_3Er_2Br_9$ and $Cs_3Er_2I_9$ absorption spectra have the same general appearance. In the iodide spectrum a high-energy broad absorption band peaking around 30 700 cm^{-1} is observed. We assign it to a $4f$-$5d$ excitation.

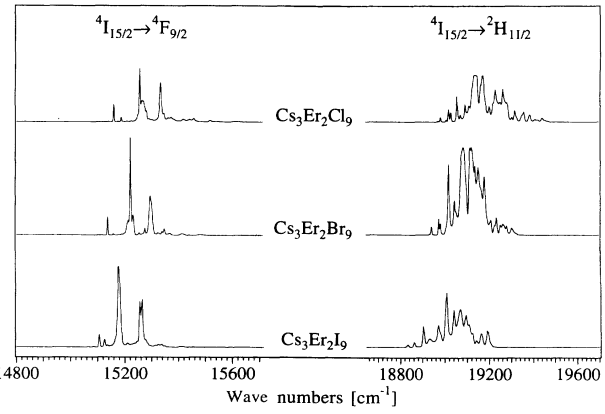

FIG. 4. Enlargement of the $^4F_{9/2}$ and $^2H_{11/2}$ absorption transitions at 13 K for $Cs_3Er_2X_9$ (X =Cl,Br,I).

TABLE II. Baricenter energies (cm^{-1}) and overall crystal-field (CF) splittings (cm^{-1}) of the multiplets in $Cs_3Er_2X_9$ (X=Cl,Br,I) derived from the 13-K absorption spectra.

Multiplet	Baricenter			Overall CF splitting		
	X=Cl	X=Br	X=I	X=Cl	X=Br	X=I
$^4I_{15/2}$	149	114	86	~320	239	~180
$^4I_{13/2}$	6612	6587	6568	195	161	133
$^4I_{11/2}$	10227	10197	10176	78	62	52
$^4I_{9/2}$	12448	12409	12400	129	113	102
$^4F_{9/2}$	15238	15206	15182	173	158	149
$^4S_{3/2}$	18286	18260	18220	33	27	17
$^2H_{11/2}$	19079	19032	18960	155	144	137
$^4F_{7/2}$	20421	20376	20319	69	67	64
$^4F_{5/2}$	22082	22040	21968	73	68	71
$^4F_{3/2}$	22445	22399	22335	43	30	21
$^2H_{9/2}$	24482	24428	24304	72	69	57

Differences in detail show up when the multiplets are magnified. Figure 4 shows the $^2H_{11/2}$ and $^4F_{9/2}$ regions for all three compounds. We note a slight redshift of the multiplet baricenters and a slight decrease of the overall splittings along the series Cl→Br→I. Both these trends are found in all the multiplets of the absorption spectrum, and Table II summarizes the results.

Room-temperature unpolarized Raman spectra of the three compounds are compared in Fig. 5. A shift of the highest-energy Raman band toward lower energy along the series Cl→Br→I is evident, as indicated by the broken line. The relevant frequencies are collected in Table III.

Room-temperature unpolarized upconversion luminescence spectra of $Cs_3Er_2X_9$ (X=Cl,Br,I) excited around 985 and 810 nm into $^4I_{11/2}$ and $^4I_{9/2}$, respectively, are shown in Figs. 6 and 7. The assignment of the various multiplets is made on the basis of a comparison with the absorption spectrum and with the upconversion luminescence in Er^{3+}-doped $CsCdBr_3$.[10,11] Figures 6 and 7 mainly serve to illustrate the different intensity distributions as we go along the series Cl→Br→I or change the excitation wavelength.

Figure 8 shows the temperature dependence of the upconversion luminescence spectra excited into $^4I_{11/2}$ for $Cs_3Er_2Cl_9$ and $Cs_3Er_2Br_9$. The overall intensity at 295 K is lower than at 10 K by factors of about 7 and 2 in $Cs_3Er_2Cl_9$ and $Cs_3Er_2Br_9$, respectively. The intensities of the $^4G_{11/2}$, $^4F_{7/2}$, and $^2H_{11/2}$ transitions are relatively higher at 295 K than at 10 K in both compounds.

Figure 9 shows upconversion excitation spectra at 12 K of $Cs_3Er_2Cl_9$ in the $^4I_{11/2}$ region for various luminescence transitions. All the spectra are very similar, indicating that the first excitation step is the same. There is excellent agreement between the $^4I_{15/2}\rightarrow{}^4I_{11/2}$ line positions measured at 13 K in absorption and excitation.

Figure 10 shows σ-polarized absorption spectra of $Cs_3Er_2Br_9$ and $Cs_3Lu_2Br_9$:1%Er^{3+} at 13 K for the transitions to the lowest four crystal-field levels (0′,1′,2′,3′) of $^4I_{13/2}$. In $Cs_3Er_2Br_9$ we observe a splitting of $^4I_{13/2}(3')$ and $^4I_{13/2}(4')$ as well as a broadening of all the lines compared to $Cs_3Lu_2Br_9$:1%Er^{3+}.

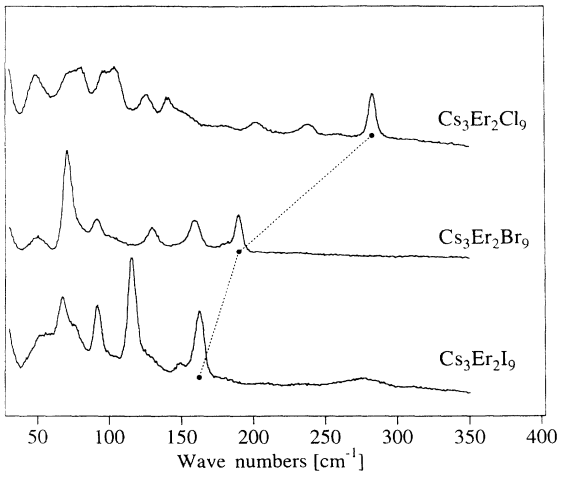

FIG. 5. Unpolarized Raman spectra at 295 K, excited at 590.6 nm, for $Cs_3Er_2X_9$ (X=Cl,Br,I). The broken line indicates the variation of the highest-energy vibration frequency.

TABLE III. The highest vibrational energies $\hbar\omega_{max}$ (cm^{-1}) for three series of lattices. p is the number of vibrational quanta $\hbar\omega_{max}$ required to bridge the $^4F_{7/2}$-$^2H_{11/2}$ energy gap of approximately ΔE=1200 cm^{-1}.

X	$Cs_3Er_2X_9$	Cs_2NaYX_6:Er^{3+}	K_2LaX_5:Er^{3+}
		$\hbar\omega_{max}$	
Cl	285[a]	260[b]	232[d]
Br	190[a]	160[b]	164[d]
I	160[a]	127[c]	
		p	
Cl	4.2	4.6	5.2
Br	6.3	7.5	7.3
I	7.5	9.4	

[a]This work.
[b]From Ref. 34.
[c]From Ref. 35.
[d]From Ref. 23.

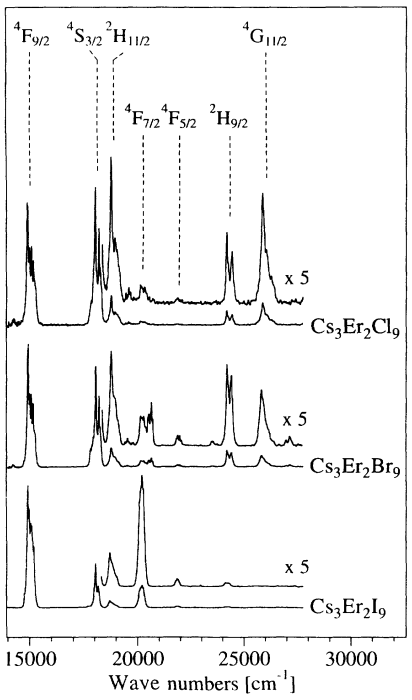

FIG. 6. Unpolarized upconversion luminescence spectra at 295 K of $Cs_3Er_2X_9$ (X=Cl,Br,I) for $^4I_{11/2}$ excitation at 982.3, 984.7, and 985.8 nm, respectively. The ordinate scales are different. The assignments denote the initial states of transitions to the $^4I_{15/2}$ ground state.

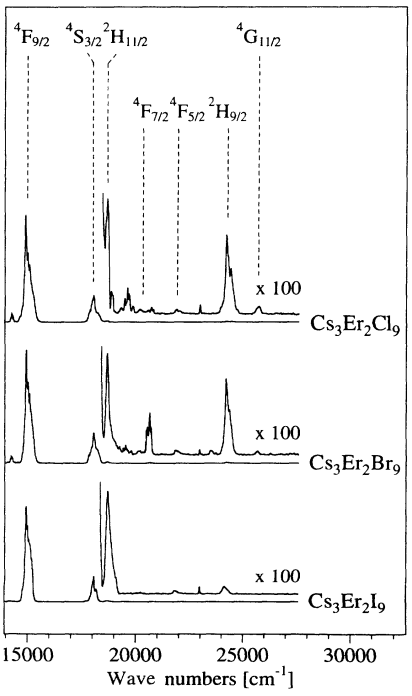

FIG. 7. Same as Fig. 6, but for $^4I_{9/2}$ excitation at 809.3, 807.4, and 808.5 nm, respectively.

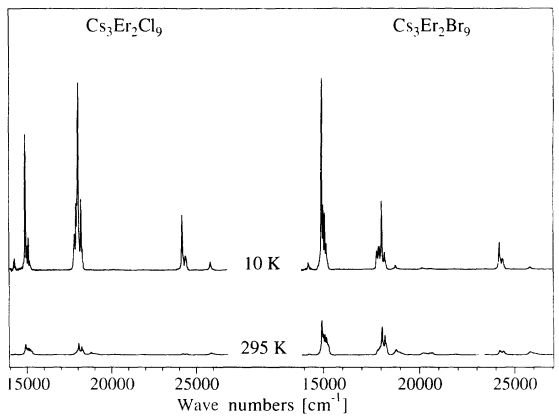

FIG. 8. Temperature dependence of the unpolarized upconversion luminescence spectra excited at 982.3 and 984.7 nm for $Cs_3Er_2Cl_9$ and $Cs_3Er_2Br_9$, respectively.

In Fig. 11, π-polarized absorption spectra of $Cs_3Er_2Br_9$ and $Cs_3Lu_2Br_9$:1%Er^{3+} at 13 K for the $^4I_{15/2}\rightarrow{}^4D_{5/2}$ and $^4I_{15/2}\rightarrow{}^4D_{7/2}$ transitions in the UV spectral region are compared. Whereas in $Cs_3Lu_2Br_9$:1%Er^{3+} we only observe the pure crystal-field transitions, there are many additional lines in $Cs_3Er_2Br_9$ which are shifted to higher energy with respect to the origins.

IV. DISCUSSION

A. Vibrational frequencies and multiphonon relaxation

The highest-energy vibrations are thought to be the most important accepting modes in multiphonon-relaxation processes. This is based on the energy-gap law, according to which the multiphonon-relaxation rate constant k_{mp} decreases exponentially with the number of phonons p required to bridge the energy gap between two electronic states:[22]

$$k_{mp}=Ce^{-p\beta}, \tag{1}$$

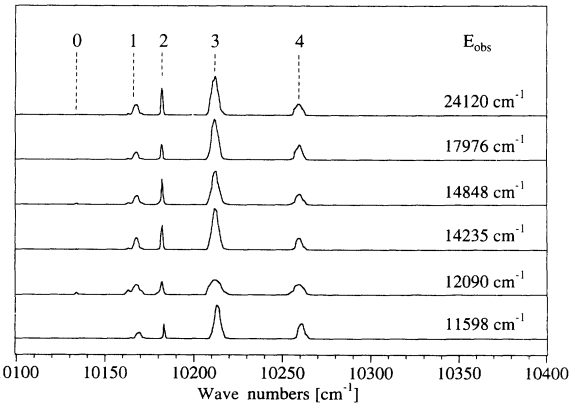

FIG. 9. Upconversion excitation spectra of $Cs_3Er_2Cl_9$ at 12 K in the region of the $^4I_{11/2}$ excitation monitoring various visible luminescence transitions.

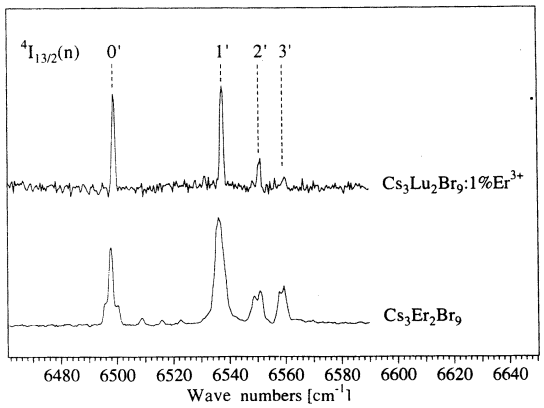

FIG. 10. σ-polarized $^4I_{15/2}(0)\rightarrow{}^4I_{13/2}(0',\ldots,3')$ absorption spectra of $Cs_3Er_2Br_9$ and $Cs_3Lu_2Br_9$:1%Er^{3+} at 13 K.

where C and β are positive-definite constants characteristic of the material. For our discussion here, we select the highest-energy vibrations which are easily identified in the Raman spectra of Fig. 5. In Table III their energies are compared with the highest-energy vibrations in the octahedral $[ErX_6]^{3-}$ species in Cs_2NaYX_6:Er^{3+}. In the latter these are the totally symmetric stretching vibrations, which do not involve any motion of the Er^{3+} ion. The situation is different in the dimer compounds because the octahedral coordination is very strongly trigonally distorted. In addition, three halide ions have a bridging function between the two octahedra, and any vibration in the $[Er_2X_9]^{3-}$ dimer involves some change of the Er^{3+}-Er^{3+} distance. As a consequence, the highest-energy vibrational frequencies in $[Er_2X_9]^{3-}$ are shifted by 25–35 cm^{-1} to higher energy with respect to the corresponding modes in the $[ErX_6]^{3-}$ octahedra.

The most intense upconversion luminescence transitions at 295 K in all the spectra of Figs. 6 and 7 are $^4S_{3/2}\rightarrow{}^4I_{15/2}$ and $^4F_{9/2}\rightarrow{}^4I_{15/2}$, with the latter dominating all the other transitions for the $^4I_{9/2}$ excitation. This behavior is in contrast to diluted Er^{3+}-doped lattices, in which the behavior very much depends on the chemical composition. In the Er^{3+}-doped bromide lattices $CsCdBr_3$,[10,11] K_2LaBr_5,[23] and $Cs_3Lu_2Br_9$,[24] the $^4F_{7/2}$ luminescences dominate the upconversion spectrum after $^4I_{11/2}$ excitation and the $^2H_{9/2}$ luminescences are dominant after $^4I_{9/2}$ excitation. In the Er^{3+}-doped chloride lattices Cs_2NaYCl_6 (Ref. 25) and K_2LaCl_5 (Ref. 23) as well as fluoride[26] lattices, the $^4S_{3/2}$ luminescence is usually dominant after $^4I_{11/2}$ excitation, with no and negligible contributions, respectively, from $^4F_{7/2}$ and $^4F_{9/2}$.

In oxide, fluoride, and chloride host lattices, the high phonon energies are thought to be responsible for the quenching of the $^4F_{7/2}$ luminescence by multiphonon relaxation to $^2H_{11/2}$ and $^4S_{3/2}$. The energy gap between $^4F_{7/2}$ and $^2H_{11/2}$ is approximately 1200 cm^{-1}, so that the number of vibrational quanta p in Eq. (1) is roughly 2, 3, and 5, respectively. In Table III the highest-energy vibrations of $Cs_3Er_2X_9$ and Cs_2NaYX_6 (X=Cl,Br,I) as well as K_2LaX_5 (X=Cl,Br) are collected, and the number of vibrational quanta p required for the $^4F_{7/2}\rightarrow{}^2H_{11/2}$ multiphonon relaxation is given. In bromide and iodide lattices the p values are roughly 7 and 8–9, respectively. As a consequence, the $^4F_{7/2}\rightarrow{}^2H_{11/2}$ multiphonon relaxation rates are slowed down by orders of magnitude. $^4F_{7/2}$ luminescence becomes competitive, as observed in diluted bromide systems. The relaxation behavior of the undiluted title compounds must therefore be dominated by other processes. These are very competitive cross-relaxation processes resulting from the dimeric nature and the undiluted character of these compounds. The importance of such processes, which will be further discussed in Sec. IV D 2, is also seen in the low intensity of the $^2H_{9/2}$ band for all three compounds in Fig. 7.

The $^2H_{9/2}$ luminescences are conspicuously weak in the iodide spectra of Figs. 6 and 7. The reason is a low-lying $4f$-$5d$ excited state which successfully competes with the $^2H_{9/2}$ luminescence. In Fig. 12 we show the

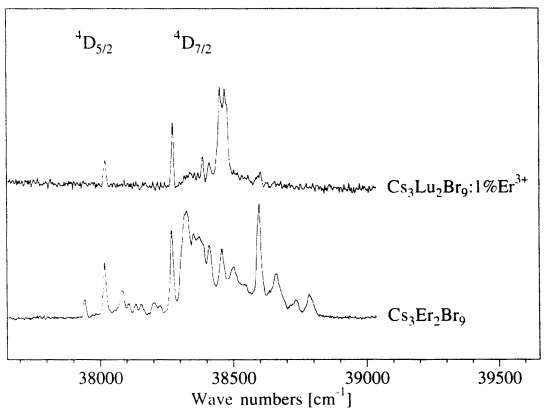

FIG. 11. π-polarized absorption spectra of $Cs_3Er_2Br_9$ and $Cs_3Lu_2Br_9$:1%Er^{3+} at 13 K for the $^4I_{15/2}\rightarrow{}^4D_{5/2}$ and $^4I_{15/2}\rightarrow{}^4D_{7/2}$ transitions.

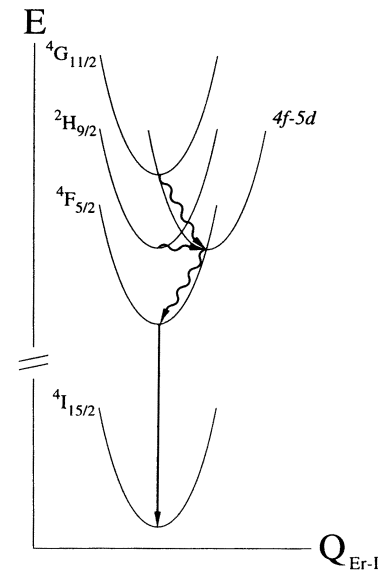

FIG. 12. Schematic configurational-coordinate diagram of some selected excited states in $Cs_3Er_2I_9$. The curly arrows indicate nonradiative relaxation pathways.

simplest configurational-coordinate diagram that accounts for this $^2H_{9/2}$ quenching. Excited states deriving from a $(4f)^{10}(5d)^1$ electron configuration are displaced along a totally symmetric Er-I configurational coordinate. This is a result of the antibonding character of the $5d$ electron. As indicated in the figure, there exist efficient nonradiative pathways from $^4G_{11/2}$ and $^2H_{9/2}$ down to $^4F_{5/2}$ via the displaced $4f$-$5d$ excited state.

B. Multiplet energies

Energies of f-f transitions are considered to be independent of the chemical nature of the crystal lattice in a first-order approximation. Our absorption and luminescence spectra confirm that this is a very good approximation (see Figs. 3, 4, 6, and 7 and Table II). However, since we have the unique opportunity to compare energies along the series Cl→Br→I without changing the structure, we can attribute the observed small redshifts of the f-f multiplet baricenters along Cl→Br→I to the chemical variation.

The covalency of the Er-X bond increases along the series Cl→Br→I. As a consequence, the orbital wave functions describing the unpaired electrons are more delocalized onto the ligands for X=I than for X=Cl. On the one hand, this leads to a reduction of the electron-repulsion parameters and thus the energies of the ^{2S+1}L manifolds. On the other hand, as is very well known for transition-metal-ion systems,[27] it leads to a reduction of the orbital angular momentum and thus to a reduction of the spin-orbit-coupling matrix elements. The combination of the two effects gives an overall small decrease of multiplet energies along Cl→Br→I, which is clearly seen in Table II.

The reduction of both electron repulsion and spin-orbit coupling along Cl→Br→I can be shown for the ^4F manifold. From Table II the baricenters for the ^4I and ^4F manifolds can be calculated. For Cl→Br and Br→I we find a decrease of the ^4I-^4F splitting of 0.05% and 0.24%, respectively, which is due to the decreasing electron repulsion along Cl→Br→I. For Cl→Br and Br→I a decrease of 0.20% and 0.56%, respectively, is found for the $^4F_{9/2}$-$^4F_{3/2}$ splitting, which is a result of the decreasing spin-orbit coupling along Cl→Br→I. The two effects tend to cancel for the lowest state of a given manifold, whereas for the highest states they add up. Thus, the observed redshift of $^4F_{9/2}$ along Cl→Br→I is significantly smaller than the redshift of the higher states $^4F_{7/2}$, $^4F_{5/2}$, and $^4F_{3/2}$ (see Table II). In order to gain a deeper insight into the physics of these energy shifts, we will attempt to determine and analyze the crystal-field energies of Er^{3+} diluted into the $Cs_3Lu_2X_9$ (X=Cl,Br,I) lattices.

C. Crystal-field splittings

We do not attempt to determine the crystal-field splittings of all the f-f excitations in this paper. Rather, we follow the crystal-field splitting of a given state along the series Cl→Br→I and try to rationalize it. We have chosen the $^4F_{9/2}$ state, and the experimental splittings derived from the highly resolved absorption spectra are collected in Table IV. We observe a general reduction of all the relative crystal-field energies along Cl→Br→I, the reduction of the total splitting being 8.7% and 5.7% for Cl→Br and Br→I, respectively. This reduction is not isotropic, as illustrated by the increasing crystal-field energy ratios $E(4')/E(n)$ (n=1′,2′,3′) shown at the bottom of Table IV.

The observed crystal-field splitting within the $^4F_{9/2}$ multiplet can be described by the effective Hamiltonian

$$\hat{H}_{C_{3v}} = B_2\hat{O}^0_2 - \tfrac{2}{3}B_4(\hat{O}^0_4 - 20\sqrt{2}\hat{O}^3_4) + \frac{16}{9}B_6\left[\hat{O}^0_6 + \frac{35\sqrt{2}}{4}\hat{O}^3_6 + \frac{77}{8}\hat{O}^6_6\right], \quad (2)$$

where the B_i (i=2,4,6) are crystal-field parameters and the $\hat{O}^j_i$ are operator equivalents.[28] Equation (2) reproduces the observed $^4F_{9/2}$ crystal-field splittings to within 1 cm^{-1}. The fit parameter values are included in Table IV. Along the series Cl→Br→I we observe a decrease of the parameters $|B_2|$ and $|B_6|$ and an increase of $|B_4|$. This nonuniform trend is a reflection of the observed anisotropy in the reduction of crystal-field splittings. The observed increase of the $E(4')/E(n)$ (n=1′,2′,3′) ratios can only be reproduced by an increase of the $|B_4|$ param-

TABLE IV. Experimental and calculated (equal to within 1 cm^{-1}) crystal-field splittings of $^4F_{9/2}$ (cm^{-1}), crystal-field parameters B_i (cm^{-1}) calculated from Eq. (2), and ratios of crystal-field energies $E(4')/E(n)$ (n=1′,2′,3′) for the series $Cs_3Er_2X_9$ (X=Cl,Br,I).

	$Cs_3Er_2Cl_9$	$Cs_3Er_2Br_9$	$Cs_3Er_2I_9$
$^4F_{9/2}$ (4′)	173	158	149
(3′)	111	94	77
(2′)	96	85	72
(1′)	27	23	20
(0′)	0	0	0
B_2	−1.25	−1.06	−0.866
B_4	3.68×10^{-3}	5.02×10^{-3}	7.95×10^{-3}
B_6	-4.76×10^{-4}	-4.32×10^{-4}	-3.98×10^{-4}
$E(4')/E(3')$	1.56	1.68	1.94
$E(4')/E(2')$	1.80	1.86	2.07
$E(4')/E(1')$	6.41	6.87	7.45

eter along Cl→Br→I. Since Eq. (2) is an effective Hamiltonian, we should be careful not to overinterpret this result, and we feel that any conclusions concerning structure-energy relationships are not possible at this level of description.

D. Interactions within and between dimers

1. Spectroscopic effects

The crystal-field levels of $Cs_3M_2Br_9$ ($M=Tb^{3+}$, Ho^{3+}, Dy^{3+}, Yb^{3+}) are split by up to 4 cm^{-1} as a result of exchange interactions within the dimers.[16–18,28] Evidence for similar splittings in the title compounds is provided in Fig. 10, where part of the $^4I_{15/2}\rightarrow{}^4I_{13/2}$ absorption spectrum of $Cs_3Er_2Br_9$ is compared with the corresponding spectrum of $Cs_3Lu_2Br_9$:1%Er^{3+}. Due to the limited instrumental resolution the lines are not fully resolved, but for some lines we observe a splitting in the undiluted sample. Similar effects can be observed in the spectra of $Cs_3Er_2Cl_9$ and $Cs_3Er_2I_9$. Since each crystal-field level, both in the ground and excited states, is expected to split into a multitude of components, the resulting splitting pattern is very complicated and could not be resolved even with higher instrumental resolution. The effect is an overall broadening of most of the lines in the concentrated compounds. Exchange splittings within the dimers are expected to decrease along the series Cl→Br→I. In the related $Cs_3Yb_2X_9$ compounds the decrease between the chloride and the bromide is about 10%.[18]

An additional broadening, although significantly smaller, is expected from interactions between the dimers in the crystal. The closest Er^{3+}-Er^{3+} distances between neighboring dimers range from 5.5 Å in the chloride to 8.2 Å in the iodide (see Table I). In Er^{3+}-doped $CsCdBr_3$, where the closest Er^{3+}-Er^{3+} separation is 6.0 Å, dimer splittings up to 0.3 cm^{-1} have been observed.[29] In the pure title compounds, therefore, the optical transitions have an excitonic character, with exciton bandwidths of the order of 0.1–0.5 cm^{-1}. These exciton bandwidths may represent the ultimate limiting factor in resolving the dimer splittings discussed above.

In addition to energy splittings the magnetic interactions can lead to cooperative electronic transitions. In these a crystal-field excitation on one Er^{3+} ion of a dimer can couple to a crystal-field excitation on the partner Er^{3+} ion, thus leading to an excited state whose energy is the sum of the individual transition energies. We have found evidence for this dimer mechanism in a one-dimensional Pr^{3+} acetate and in $Cs_3Yb_2Br_9$.[30,31] Evidence for cooperative excitations is also found in the title compounds. They are most easily recognized in Fig. 11, where we compare the $^4D_{5/2}$ and $^4D_{7/2}$ transitions in $Cs_3Er_2Br_9$ with the corresponding $Cs_3Lu_2Br_9$:1%Er^{3+} transitions. There are numerous lines in the $Cs_3Er_2Br_9$ spectrum which have no counterpart in the diluted system and which are blueshifted from the pure crystal-field transitions. The spectrum has not been fully analyzed, but the additional lines in the $Cs_3Er_2Br_9$ spectrum are blueshifted in a range which roughly corresponds to the overall splitting of the $^4I_{15/2}$ ground state. However, not all of the additional lines can be explained by this mechanism; some must be due to vibronic transitions. It has been observed in other systems that the intensity of vibronic sidebands increases with increasing rare-earth-ion concentration.[32]

2. Upconversion and cross relaxation

References 1 and 2 are early reviews of the various mechanisms for upconversion in rare-earth metal-ion systems. Due to the close proximity of Er^{3+} ions within and between the dimers in the title compounds, the dominant mechanism in our systems is one in which excitation energy is transferred nonradiatively from one excited Er^{3+} center to its neighbor. Such processes can occur by an exchange or an electric multipole-multipole mechanism. Since we have spectroscopic evidence for relatively strong exchange interactions within the dimers, we expect the exchange mechanism to play an important part in the corresponding nonradiative processes. No overlap of the electronic wave functions is needed for electric dipole-dipole induced transfer processes. We expect them to become dominant as we go to longer Er^{3+}-Er^{3+} distances between the dimers (cf. Table I). There are no halogen ions bridging neighboring dimers, and they are separated by the Cs^+ ions. The two types of mechanisms cannot easily be distinguished, but our dimer systems provide a great deal of evidence for the importance of both intra- and interdimer excitation-transfer processes. In the following qualitative discussion we focus on the upconversion trends observed along the series Cl→Br→I. A more detailed analysis of excited-state dynamics in $Cs_3Er_2Br_9$ and $Cs_3Lu_2Br_9$:1%Er^{3+} will be given elsewhere.[33]

NIR-to-visible upconversion does occur in all three compounds at all temperatures between 10 and 295 K. As seen in Figs. 6 and 7 the $^4F_{9/2}\rightarrow{}^4I_{15/2}$ transition is among the most intense for both excitations and at all temperatures. This is in contrast to the upconversion behavior of Er^{3+}-doped $CsCdBr_3$ and K_2LaBr_5, where the $^4F_{9/2}$ intensity is insignificant for $^4I_{11/2}$ excitation.[10,11,23] We ascribe the high steady-state population of $^4F_{9/2}$ in our undiluted dimer compounds to highly efficient cross-relaxation processes depleting the higher-energy states. Since multiphonon-relaxation processes are relatively unimportant, at least in the bromide and iodide lattices, excitation-energy migration between dimers is likely to occur within the lifetimes of all the excited states. This increases the probability of cooperative nonradiative processes such as upconversion and cross relaxation, which involve more than one $[Er_2X_9]^{3-}$ dimer. In the following discussion we will use Fig. 13, which illustrates the most likely cross-relaxation mechanisms. Some of the mechanisms are not exactly resonant, but the excess energy can be released as phonon energy into the lattice.

The processes 13(a) and 13(b) can account for the observed concentration quenching down to $^4S_{3/2}$ and $^4F_{9/2}$, respectively, after $^4I_{9/2}$ excitation and $^2H_{9/2}$ upconversion [Fig. 1(b)]. After $^4I_{11/2}$ excitation and $^4F_{7/2}$ upconversion [Fig. 1(a)] the $^4F_{9/2}$ state can be reached by the

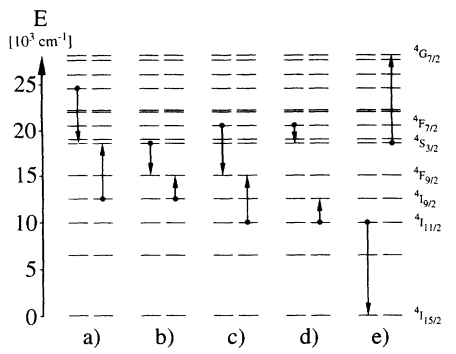

FIG. 13. Cross-relaxation and upconversion mechanisms discussed in Sec. IV D 2. Baricenter energies are used for the energy diagram.

one-step process 13(c).

The $^4S_{3/2} \rightarrow {}^4I_{15/2}$ transition is the dominant upconversion luminescence band in fluoride lattices such as $YLiF_4$ and BaY_2F_8. It also has high intensity in the title compounds for both $^4I_{11/2}$ and $^4I_{9/2}$ excitation. In the fluorides, the high $^4S_{3/2}$ population is mainly the result of fast multiphonon-relaxation processes from the relatively close-lying higher excited states, particularly $^4F_{7/2} \rightarrow {}^2H_{11/2} \rightarrow {}^4S_{3/2}$. As discussed in Sec. IV A, this might still be possible for $Cs_3Er_2Cl_9$, but it is unlikely for the bromide and iodide due to the lower phonon energies. The most likely mechanisms are cooperative cross relaxations, such as process 13(a) after $^4I_{9/2}$ excitation and process 13(d) after $^4I_{11/2}$ excitation. The relative importance of $^4S_{3/2}$ decreases along Cl→Br→I (see Figs. 6 and 7). It appears that processes such as 13(c) which bypass $^4S_{3/2}$ are more efficient in the iodide.

Upconversion luminescence from $^4G_{11/2}$ is quite prominent at room temperature in $Cs_3Er_2Cl_9$ and $Cs_3Er_2Br_9$ after $^4I_{11/2}$ excitation (Fig. 6). This is in contrast to fluoride and oxide host lattices. We ascribe the relatively high $^4G_{11/2}$ steady-state population to a high efficiency of cooperative processes such as upconversion according to Fig. 1(a) followed by cross relaxation 13(d) and upconversion 13(e). These processes are favored in the undiluted compounds due to the excitonic nature of the transitions. The relative weakness of $^2H_{9/2}$ upconversion luminescence transitions after $^4I_{9/2}$ excitation for all three compounds is particularly striking (see Fig. 7). It is in contrast to the behavior observed for Er^{3+}-doped $CsCdBr_3$ and K_2LaBr_5, where the $^2H_{9/2}$ transitions dominate the corresponding upconversion spectrum.[10,11,23] This difference can again be ascribed to cooperative cross-relaxation processes such as 13(a) which are more efficient in the undiluted materials.

V. CONCLUSIONS

The upconversion luminescence behavior of the title compounds is different from the behavior of Er^{3+}-doped oxide and fluoride materials on the one hand, but it is also different from Er^{3+} doped in low concentrations into chloride and bromide lattices. In bromide and iodide, and to a lesser degree, in chloride lattices the multiphonon-relaxation rate constants are reduced by orders of magnitude with respect to oxide and fluoride lattices. This is due to the lower phonon energies in the heavier halide lattices, and it leads to completely different excited-state dynamics and steady-state populations. In addition, the competition between the various radiative and nonradiative relaxation processes is affected by the dimeric nature of the compounds and the relatively close contacts between neighboring dimers in the lattice. The probability of nonradiative energy-transfer processes such as upconversion and cross relaxation is strongly enhanced by the close proximity of Er^{3+} ions within the $[Er_2X_9]^{3-}$ pairs. Cooperative upconversion and cross-relaxation processes involving more than one dimer become important because energy transfer between neighboring dimers is also possible. As a result, upconversion and cross-relaxation processes dominate not only the multiphonon relaxation but also the radiative luminescence. The net result of this "concentration quenching" is a high population of the low-lying states in the near infrared.

ACKNOWLEDGMENTS

Part of this research was carried out while one of us (H.U.G.) was at the Hughes Research Laboratories, Malibu, CA. It is a pleasure to acknowledge valuable discussions with G. C. Valley, M. Robinson, and N. Cockroft and the excellent technical support by J. E. Brown, R. A. Cronkite, K. C. Fuller, and N. Furer. This work was partially supported by the Swiss National Science Foundation.

[1]F. E. Auzel, Proc. IEEE **61**, 758 (1973).
[2]J. C. Wright, Top. Appl. Phys. **15**, 239 (1976).
[3]D. L. Dexter, J. Chem. Phys. **21**, 836 (1953).
[4]R. J. Thrash and L. F. Johnson (unpublished).
[5]W. Lenth and R. M. Macfarlane, Opt. Photon. News **3**, 8 (1992).
[6]A. J. Silversmith, W. Lenth, and R. M. Macfarlane, Appl. Phys. Lett. **51**, 1977 (1987).
[7]W. Lenth, A. J. Silversmith, and R. M. Macfarlane, in *Advances in Laser Science III*, edited by A. C. Tam, J. L. Gole, and W. C. Stwalley, AIP Conf. Proc. No. 172 (AIP, New York, 1988), p. 8.
[8]R. A. McFarlane, Appl. Phys. Lett. **54**, 2301 (1989).
[9]T. Hebert, R. Wannemacher, W. Lenth, and R. M. Macfarlane, Appl. Phys. Lett. **57**, 1727 (1990).
[10]N. J. Cockroft, G. D. Jones, and D. C. Nguyen, Phys. Rev. B **45**, 5187 (1992).
[11]R. N. Schwartz and R. A. McFarlane, OSA Proc. Adv. Solid State Lasers **13**, 384 (1992).
[12]G. L. McPherson, A. Ghavari, and S. L. Meyerson, Chem. Phys. **165**, 361 (1992).
[13]G. Meyer, Z. Anorg. Allg. Chem. **455**, 140 (1978).

[14]G. Meyer, Prog. Solid State Chem. **14**, 141 (1982).
[15]S. H. Wang, S. M. Zuo, H. Eick, K. Krämer, and G. Meyer, J. Less Common Met. **155**, 45 (1989).
[16]A. Furrer, H. U. Güdel, H. Blank, and A. Heidemann, Phys. Rev. Lett. **62**, 210 (1989).
[17]A. Furrer, H. U. Güdel, E. R. Krausz, and H. Blank, Phys. Rev. Lett. **64**, 68 (1990).
[18]H. U. Güdel, A. Furrer, and H. Blank, Inorg. Chem. **29**, 4081 (1990).
[19]G. Meyer, *Synthesis of Lanthanide and Actinide Compounds* (Kluwer, Dordrecht, 1991).
[20]K. Krämer, Ph.D. thesis, University of Giessen, Germany, 1991.
[21]IGOR Software, WaveMetrics, Lake Oswego, Oregon.
[22]L. A. Riseberg and H. W. Moos, Phys. Rev. **174**, 429 (1968).
[23]K. Krämer and H. U. Güdel, in *Proceedings of the 20th Rare Earth Research Conference,* Monterey, California, 1993 [J. Alloys Compounds (to be published)].
[24]M. P. Hehlen, K. Krämer, and H. U. Güdel, in *Proceedings of the 1993 International Conference on Luminescence,* Storrs, Connecticut, 1993 [J. Lumin. (to be published)].
[25]H. U. Güdel and R. A. McFarlane (unpublished).
[26]A. A. Kaminskii, S. E. Sarkisov, F. Below, and H. J. Eichler, Opt. Quantum Electron. **22**, 595 (1990).
[27]J. S. Griffith, *The Theory of Transition Metal Ions* (Cambridge University Press, Cambridge, England, 1961).
[28]A. Furrer, H. U. Güdel, and J. Darriet, J. Less Common Met. **111**, 223 (1985).
[29]N. J. Cockroft (private communication).
[30]M. P. Hehlen, H. Riesen, and H. U. Güdel, Inorg. Chem. **30**, 2273 (1991).
[31]M. P. Hehlen and H. U. Güdel, J. Chem. Phys. **98**, 1768 (1993).
[32]C. M. Donegá, M. J. G. Crombag, A. Meijerink, and G. Blasse, in *Proceedings of the 1993 International Conference on Luminescence,* Storrs, Connecticut, 1993 (Ref. 24).
[33]M. P. Hehlen, G. Frei, and H. U. Güdel (unpublished).
[34]M. Choca, J. R. Ferraro, and K. Nakamoto, Coord. Chem. Rev. **12**, 295 (1974).
[35]G. Meyer, Z. Naturforsch. Teil B **35**, 394 (1980).

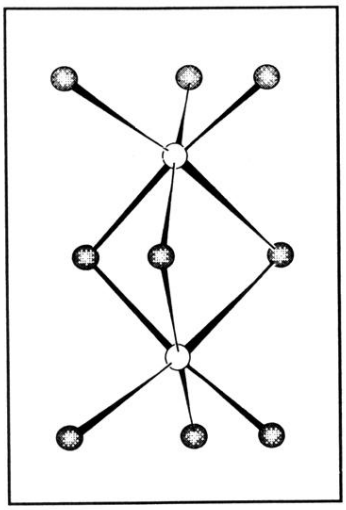

FIG. 2. Dimer structure of $[Er_2X_9]^{3-}$.